

1 Upper tropospheric circulation associated with Kelvin waves propagating
2 through the Madden-Julian oscillation

3 Crizzia Mielle De Castro

5 ABSTRACT: This study investigates the spatial and temporal evolution of upper tropospheric
6 dynamics associated with a Kelvin wave propagating through the Madden-Julian oscillation's
7 (MJO) active convection. To examine upper tropospheric dynamics, this study looks at 20-day
8 time-lagged composites of outgoing longwave radiation (OLR) with 200 *mb* geopotential height,
9 200 *mb* winds, 300 *mb* specific humidity, and 200 *mb* temperature anomalies. Only days with the
10 real-time multivariate MJO (RMM) index at phase 3, and strong Kelvin waves passing through (1)
11 80°E, and (2) 110°E were considered. Monte Carlo experiments determined the time and location
12 of the statistically significant effects of the Kelvin wave. This study found that the Kelvin wave
13 propagating with the MJO appear as a small strong OLR signal embedded within a larger weaker
14 OLR signal. In the upper troposphere, a low geopotential height coincided with easterlies west of
15 the Kelvin wave, and vice versa to the east. The Kelvin wave passing through 110°E moistened and
16 warmed the west upper troposphere much earlier than the Kelvin wave passing through 80°E. The
17 tilted vertical structure of the Kelvin wave manifested in the shifted statistically significant time
18 and locations of the composites. To better observe this tilt, future work will look at other pressure
19 levels, particularly the lower and middle troposphere.

20 **1. Introduction**

21 *a. Background on Kelvin waves and the Madden-Julian oscillation*

22 Convectively-coupled equatorial waves act as organized convective disturbances that propagate
23 along the equator, thereby controlling rainfall and wind patterns across the tropics (Kiladis et al.
24 2009). The solutions to the shallow water equations on an equatorial β -plane from Matsuno (1966)
25 characterize the spatial and temporal propagation of equatorial waves. Of particular interest in
26 this study are Kelvin waves, eastward moving convective disturbances with an average 15-day
27 period, phase speeds of $15 - 20 \text{ m/s}$, and horizontal structures at around $3,300 - 6,600 \text{ km}$ in scale
28 (Wallace and Kousky 1968).

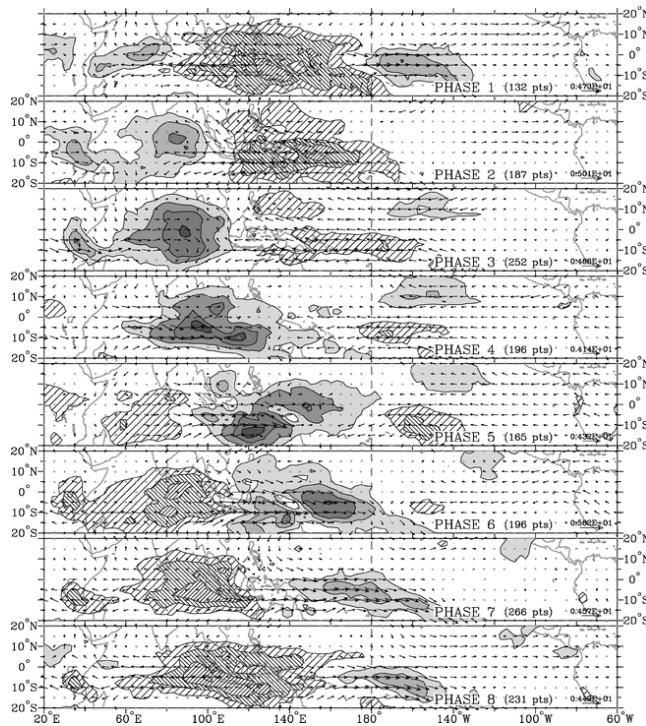


FIG. 1: Composite OLR (shaded) and 850 mb wind vector anomalies for 8 RMM phases. Solid shading denotes positive OLR anomalies, while hatching denotes negative OLR anomalies. Figure from Wheeler and Hendon (2004).

29 Nakazawa (1988) observed the fast-moving synoptic scale Kelvin waves as part of a slower-
30 moving planetary scale convective structure known as the Madden-Julian oscillation (MJO). The
31 MJO follows a 40-50 day period, eastward phase speeds of $4 - 8 \text{ m/s}$, and horizontal structures
32 at around $10,000 \text{ km}$ in scale (Madden and Julian 1994). The eastward propagation of the MJO

can be described using the real-time multivariate MJO (RMM) index developed by Wheeler and Hendon (2004). The RMM index indicates the MJO's phase from 1-8 (illustrated in Fig. 1). For example, at RMM phase three, the MJO active convection occurs over the Indian ocean, and the MJO suppressed convection occurs over the west Pacific ocean.

b. Statement of the Problem

My current research works with the hypothesis that the vertical structure of circulation due to Kelvin waves depends on whether the Kelvin wave propagates through active or suppressed MJO convection. To work towards testing this hypothesis, this study looks at upper tropospheric dynamics associated with Kelvin waves propagating through the MJO's active convection. Two cases were investigated: an active Kelvin wave passing through (1) 80° E and (2) 110° E during the RMM phase 3. This study uses time-lagged composites of geopotential height, wind, specific humidity, and temperature to describe upper tropospheric dynamics, and outgoing longwave radiation (OLR) to describe convection. To look at the evolution of circulation patterns, this study investigates what happens 20 days before and after the event. The rest of the paper refers to *the event* as a Kelvin wave propagating through the active MJO convection. Lastly, Monte Carlo experiments were used to determine when and where the Kelvin wave's effects on circulation patterns are statistically significant.

c. Research Questions

This study aims to answer the following questions.

- How do upper tropospheric dynamics and OLR respond to a Kelvin wave propagating through the MJO's active convection?
- When and where are the effects of the Kelvin wave on circulation patterns statistically significant?

d. Significance

The MJO and Kelvin waves have been associated with tropical cyclogenesis as precursors and modulators. Schreck et al. (2012) discovered the MJO to be an important precent to tropical cyclone (TC) formation over the north Indian, south Indian, and western North Pacific TC basins.

60 They also found the strongest MJO modulation corresponded to storms associated with Kelvin
61 waves over the north Indian ocean. The MJO has also been found to promote TC formation
62 in faster moving waves (Nakazawa 1986; Aiyyer and Molinari 2008). Lastly, the MJO can act
63 as precursors to extratropical Rossby gyres (Schreck et al. 2013), which may develop into Kelvin
64 waves upon reaching the equator (Straub and Kiladis 2003). The interactions between the MJO and
65 Kelvin wave can lead to further understanding of TC formation and extratropical wave formation.
66 Thus, looking at their combined effects on atmospheric circulation patterns warrants more extensive
67 research.

68 2. Methods

69 Data

70 This study uses gridded data of daily mean OLR, 200 mb geopotential height, 200 mb winds
71 (zonal and meridional), 300 mb specific humidity, and 200 *mb* air temperature from NCEP
72 Reanalysis data provided by NOAA/OAR/ESRL PSL (Kalnay et al. 1996). All data used for
73 succeeding analyses spans from January 1979 to August 1996, and has a resolution of $2.5^\circ \times 2.5^\circ$.
74 Outgoing longwave radiation was used as a proxy for observing convection caused by equatorial
75 waves (adapting methods in Wheeler and Kiladis (1999)). Lastly, this study uses the daily RMM
76 phase data from the International Research Institution (IRI) Climate Data Library in <https://iridl.ldeo.columbia.edu/>, adapted from Wheeler and Hendon (2004).

77 The remaining methods use the anomalies of OLR, geopotential height, winds, specific humidity,
78 and temperature. To get their anomalies, this study removed the seasonal cycle from the dynamical
79 data following the methods prescribed in Roundy (2020), which uses a simple linear regression
80 model $\mathbf{Y} = \mathbf{X}\mathbf{C} + \epsilon$. Here, \mathbf{X} denotes the predictor matrix, \mathbf{C} denotes the regression coefficients,
81 \mathbf{Y} denotes the observed data, and ϵ denotes the anomalies. Assuming the seasonal cycle follows
82 peaks and troughs, \mathbf{X} contains a column of ones, and three harmonics of sine and cosine waves.
83 The following equation solves for \mathbf{C} .

$$84 \mathbf{C} = (\mathbf{X}^T \mathbf{X})^{-1} \mathbf{X}^T \mathbf{Y} \quad (1)$$

85 Thus, $\mathbf{X}\mathbf{C}$ denotes the seasonal cycle, and the anomalies are given by $\epsilon = \mathbf{Y} - \mathbf{X}\mathbf{C}$.

86 *a. Filtering Kelvin wave signals from OLR*

87 This study closely follows methods from Wheeler and Kiladis (1999) and Roundy (2020) where a
 88 2-dimensional Fourier transform was applied to OLR anomalies to obtain signals in a wavenumber-
 89 frequency spectrum. The OLR anomalies were averaged from latitudes -15° to 15° , and arranged
 90 into longitude-time arrays. The OLR anomalies were then separated into 96-day segments and win-
 91 dowed such that each segment overlaps its neighbours by 48 days. Multiplying the 2-dimensional
 92 Fourier transform of the segmented arrays by their complex conjugates gets their power spectrum.
 93 To get the background power spectrum, MATLAB's smoothing function smoothed the power spec-
 94 trum 30 times each along space and time. The original power spectrum divided by the background
 95 spectrum denotes the normalized spectrum. The t -test at $\alpha = 0.95$ with a sample size of 206
 96 determines the statistically significant signals in the normalized power spectrum, which describes
 97 at what phase speeds the detectable equatorial waves operate (illustrated in Fig. 2). The normal-
 98 ized power spectrum illustrate the following detectable equatorial waves: westward inertia-gravity
 99 (WIG) waves, eastward inertia-gravity (EIG) waves, equatorial-Rossby (ER) waves, Kelvin waves,
 100 and the MJO. This study only discusses the wave-like MJO and Kelvin waves. Kelvin waves were
 101 arbitrarily determined to propagate eastward within wavenumber 2-9 and frequency 0.05-0.33.
 102 Following a band-pass filter, all signals in the Fourier spectrum outside of this domain were then
 103 masked (set to zero). From here, applying an inverse Fourier transform on the Fourier spectrum
 104 filters the Kelvin wave OLR signals.

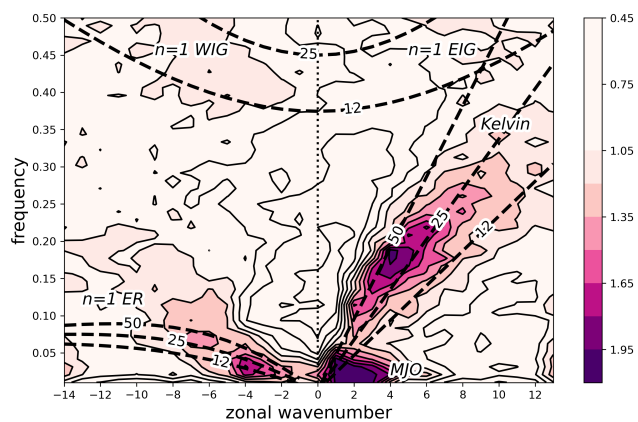


FIG. 2: Normalized power spectrum of OLR anomalies (shaded and contoured) after applying 2D Fourier transform. Dispersion curves (dashed lines) show solutions to the shallow water equations from Matsuno (1966) at different equivalent heights (12, 25, 50). Text labels denote equatorial waves.

¹⁰⁵ *b. Time-lagged composites of OLR with dynamical data*

¹⁰⁶ To observe how circulation behaves when the Kelvin wave propagates further eastward along its
¹⁰⁷ path, two base longitudes were chosen: 80°E and 110°E. Using the IRI data and filtered Kelvin
¹⁰⁸ wave OLR, all days with a Kelvin wave passing through the base longitudes at MJO RMM phase 3
¹⁰⁹ were added to a list. To get the strongest possible Kelvin wave signals, this study only considered
¹¹⁰ days from the list with negative local minimum Kelvin wave OLR below one negative standard
¹¹¹ deviation. Following these criteria, from 6453 active Kelvin wave days, 59 days for 80°E and 57
¹¹² days for 110°E remained.

¹¹³ The time-lagged composites included only OLR and dynamical data from the final list of dates.
¹¹⁴ Geopotential height, winds, specific humidity, and temperature were averaged from latitudes 5°S
¹¹⁵ to 5°N. Using a maximum lag of 20 days, the average of the OLR and dynamical data anomalies
¹¹⁶ of all days forms the composites as the lag moves backward or forward in time.

¹¹⁷ *c. Monte Carlo experiments to assess significance*

¹¹⁸ This study follows the Monte Carlo experiments on wave spectra used in Roundy (2020). The
¹¹⁹ Fourier transform of the Kelvin wave OLR time series at the base longitudes were randomized
¹²⁰ while maintaining the same power spectra. Their inverse transform acts as a randomized Kelvin
¹²¹ wave under the same RMM phase. Repeating the time-lagged procedures using different random
¹²² Kelvin wave OLRS 1000 times creates a null distribution of the dynamical data. This study observes
¹²³ the following null hypothesis: The MJO with the Kelvin wave is not statistically different from the
¹²⁴ MJO with a random wave. If the actual composite falls outside the 95% confidence interval of the
¹²⁵ null distribution, then the null hypothesis was rejected.

¹²⁶ **3. Results and Discussion**

¹²⁷ *a. Response of OLR to Kelvin waves propagating through the MJO*

¹²⁸ The plot of the OLR anomalies (see Figs. 3-5) show a very strong, small convection signal (in
¹²⁹ dark blue green) embedded in a larger weaker convection signal (in light blue green), indicating
¹³⁰ a small Kelvin wave clearly embedded within the larger MJO. The OLR signals also show the
¹³¹ weaker convection around the west Pacific ocean at 100° – 180° associated with the RMM phase

132 3. Lastly, as expected, the stronger Kelvin wave signal extends further eastward at a more eastward
 133 base longitude.

134 *b. Response of geopotential height and winds to Kelvin waves propagating through the MJO*

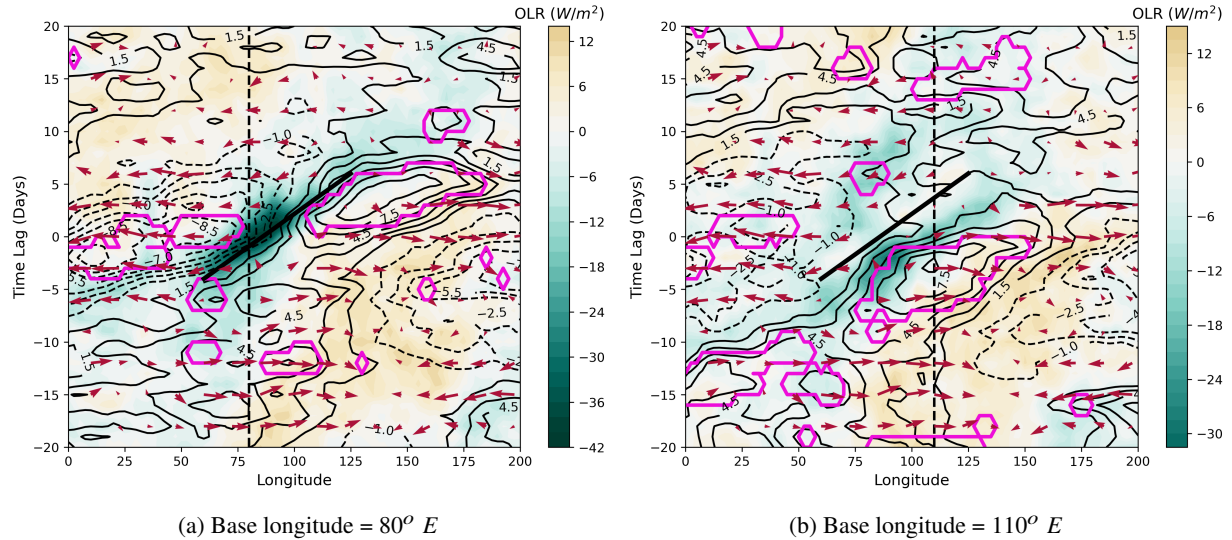


FIG. 3: OLR (shaded in W/m^2), 200 mb geopotential height (contours in $1.5 m$ intervals), and 200 mb wind field (red quivers in m/s) anomalies for a Kelvin wave passing through base longitudes (a) $80^\circ E$, and (b) $110^\circ E$ during RMM phase 3. Solid contours denote positive anomalies, while dashed contours denote negative anomalies. The dashed vertical line denotes the base longitude, and the thick diagonal line is just for reference to compare the shifted Kelvin OLR signals. Pink contours denote statistically significant regions obtained through Monte Carlo experiments.

135 The wind field anomalies (see Fig. 3) show the upper tropospheric zonal wind divergence
 136 associated with the active Kelvin wave. An anomalously low geopotential height coincides with
 137 easterlies to the west of the active Kelvin wave convection, while an anomalously high geopotential
 138 height coincides with westerlies to the east of the active Kelvin wave convection. This matches
 139 well with results presented in Kiladis et al. (2009). The contours of the positive and negative
 140 geopotential heights coincide with the negative and positive OLR, respectively, but shifted about
 141 20° eastward. Looking at the pink contours in Fig. 3a, the effects of the Kelvin wave on the
 142 geopotential height is statistically significant to the west 3-4 days before the event, and to the east
 143 4-5 days after the event. This shift in geopotential height occurs earlier in Fig. 3b (lower left pink
 144 contours) starting around 15 days before the event. The tilted vertical structure of Kelvin waves

145 (Kiladis et al. 2009) explains the shift of statistically significant regions away from the time and
 146 location of the event.

147 *c. Response of specific humidity and temperature to Kelvin waves propagating through the MJO*

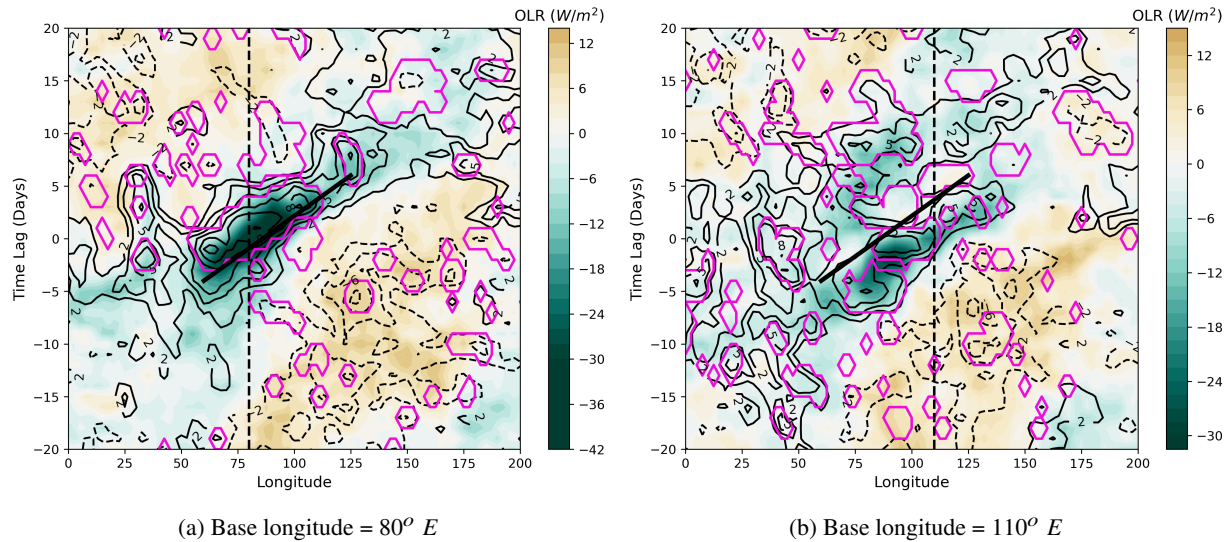


FIG. 4: Same as Fig. 3, but with 300 *mb* specific humidity anomalies (contours in $2 \times 10^{-5} \text{ kg/kg}$ intervals). Contour labels were multiplied by 1×10^5 to fit values.

148 The positive contours of the specific humidity anomalies (see Fig. 4) coincide with the active
 149 MJO signal (light blue green), and vice versa. The pink contours show that statistically significant
 150 regions of specific humidity occur during the Kelvin wave event, and some patches to the west
 151 after the event (upper left pink contours). The MJO moistens the upper troposphere before the
 152 event (wide region of black contours at lower left of Figs. 4a and 4b), until the passing Kelvin wave
 153 concentrates high water vapor along its path. As the Kelvin wave and MJO move eastward, they
 154 leave a wake of high humidity to the west that can last up to 15 days after the event (solid contours
 155 at upper left of Fig. 4).

156 Based on Kiladis et al. (2005), the active MJO can keep the upper troposphere moist up to 10
 157 days after passing, while based on Kiladis et al. (2009), active Kelvin waves can keep the upper
 158 troposphere moist up to 1.5 days after passing. Results indicate that when propagating together,
 159 the active MJO and Kelvin waves can keep the upper troposphere moist longer than on their own.
 160 The lower left pink contours appear in Fig. 4b, but not in Fig. 4a, indicating that the active Kelvin

161 wave moistens the west upper troposphere earlier (up to 15 days before the event) as it develops
 162 further eastward. Islands between the Indian ocean to the Maritime Continent along the MJO and
 163 Kelvin wave's path may account for the patchiness of the statistically significant regions.

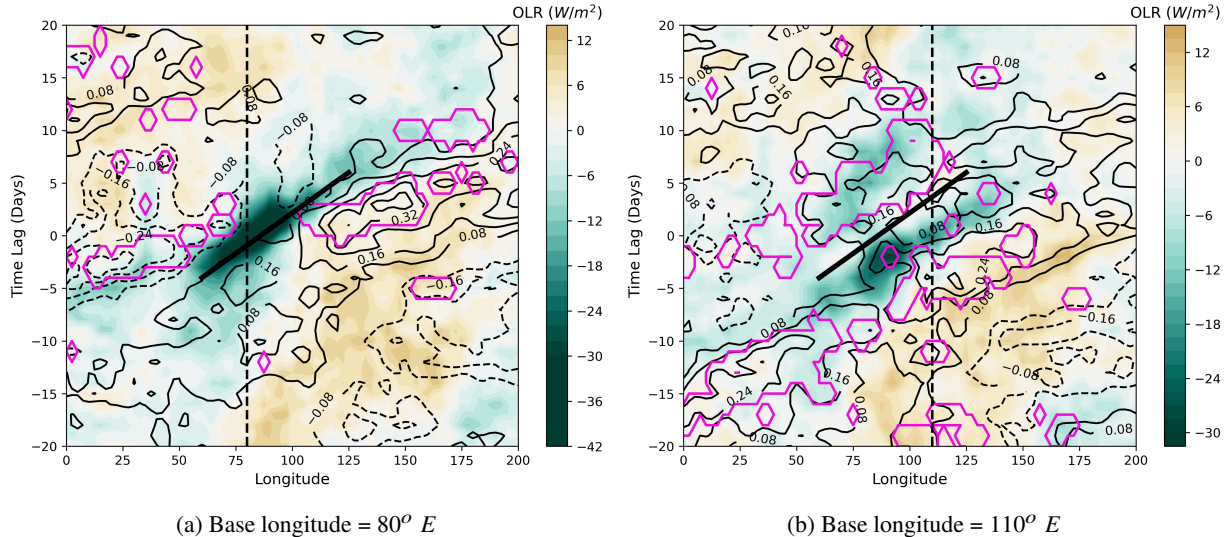


FIG. 5: Same as Fig. 3, but with 200 *mb* temperature anomalies (contours in 0.08 *K* intervals).

164 The contours of the temperature anomalies (see Fig. 5) coincide well with the contours of
 165 geopotential height anomalies, including the eastward shift and regions of statistical significance.
 166 Similar to geopotential height, the regions of statistically significant temperature at base longitude
 167 = $110^\circ E$ (see Fig. 5b) shifts eastward earlier than at base longitude = $80^\circ E$. Looking at the
 168 lower left and upper right, the temperature anomalies remain positive up to 20 days before and
 169 after the event, which can be attributed to the warm signal of the MJO's active convection around
 170 200 – 400 *mb* (Kiladis et al. 2005). Following the dashed vertical line, the upper troposphere
 171 remains anomalously warm before the event with a peak shifted eastward during the event.

172 A short cold spell occurs around 5 days before and after the event to the west (leftmost dashed
 173 contours), which can be attributed to the active Kelvin wave's thermodynamics (Kiladis et al.
 174 2009). Similar to Fig. 4, lower left pink contours appear in Fig. 5b, but not in Fig. 5a, indicating
 175 that the active Kelvin wave warms the west upper troposphere earlier (up to 18 days before the
 176 event) as it develops further eastward. The active Kelvin wave and MJO also leave a wake of
 177 anomalously high temperatures (middle pink contours in Fig. 5b) in its wake lasting up to 10 days
 178 after the event.

179 **4. Conclusions and Recommendations**

180 The active Kelvin wave propagating through the active MJO appears as a small strong region
181 of OLR signal embedded in a larger weaker region of OLR signal. As expected in the upper
182 troposphere, a low geopotential height coincides with easterlies to the west of the active Kelvin
183 wave convection, and vice versa to the east. High specific humidity in the upper troposphere
184 coincide with the active MJO convection, and vice versa. As the Kelvin wave propagates through
185 the MJO, they leave a wake of high humidity 15 days after their initialization, which is about 5 days
186 longer than the MJO alone. When further eastward along its path, the Kelvin wave also moistens
187 and warms the west upper troposphere by up to 15 days before its initialization with the MJO. The
188 shifted statistically significant time and locations of geopotential height, specific humidity, and
189 temperature illustrate the tilted vertical structure of the Kelvin wave

190 To better observe the tilted vertical structure of the Kelvin wave, future studies on Kelvin
191 wave-MJO events can be applied to different pressure levels, particularly the lower and middle
192 troposphere. Other dynamical data could also be investigated, including potential vorticity, mass
193 flux, precipitation rate, and divergence. This study only looks at an active Kelvin wave propagating
194 through the MJO's active convection. Thus, future studies could also explore a Kelvin wave
195 propagating through the MJO's suppressed convection, by changing the RMM index or the Kelvin
196 wave's base longitude.

197 **References**

- 198 Aiyyer, A., and J. Molinari, 2008: MJO and Tropical Cyclogenesis in the Gulf of Mexico and
199 Eastern Pacific: Case Study and Idealized Numerical Modeling. *Journal of the Atmospheric*
200 *Sciences*, **65** (8), 2691–2704, <https://doi.org/10.1175/2007JAS2348.1>.
- 201 Kalnay, E., and Coauthors, 1996: The NCEP/NCAR 40-Year Reanalysis Project. *Bulletin of the*
202 *American Meteorological Society*, **77** (3), 437–472, [https://doi.org/10.1175/1520-0477\(1996\)077<0437:TNYRP>2.0.CO;2](https://doi.org/10.1175/1520-0477(1996)077<0437:TNYRP>2.0.CO;2).
- 203 Kiladis, G. N., K. H. Straub, and P. T. Haertel, 2005: Zonal and Vertical Structure of the Mad-
204 den–Julian Oscillation. *Journal of the Atmospheric Sciences*, **62** (8), 2790–2809, <https://doi.org/10.1175/JAS3520.1>.

- 207 Kiladis, G. N., M. C. Wheeler, P. T. Haertel, K. H. Straub, and P. E. Roundy, 2009: Convectively coupled equatorial waves. *Reviews of Geophysics*, **47** (2), <https://doi.org/10.1029/2008RG000266>.
- 210 Madden, R. A., and P. R. Julian, 1994: Observations of the 40–50-day tropical oscillation—a review. *Monthly Weather Review*, **122** (5), 814 – 837, [https://doi.org/10.1175/1520-0493\(1994\)122<0814:OOTDTO>2.0.CO;2](https://doi.org/10.1175/1520-0493(1994)122<0814:OOTDTO>2.0.CO;2).
- 213 Matsuno, T., 1966: Quasi-geostrophic motions in the equatorial area. *Journal of the Meteorological Society of Japan. Ser. II*, **44** (1), 25–43, https://doi.org/10.2151/jmsj1965.44.1_25.
- 215 Nakazawa, T., 1986: Intraseasonal Variations of OLR in the Tropics During the FGGE Year. *Journal of the Meteorological Society of Japan. Ser. II*, **64**, 17–34, https://doi.org/10.2151/jmsj1965.64.1_17.
- 218 Nakazawa, T., 1988: Tropical super clusters within intraseasonal variations over the western pacific. *Journal of the Meteorological Society of Japan. Ser. II*, **66** (6), 823–839, https://doi.org/10.2151/jmsj1965.66.6_823.
- 221 Roundy, P. E., 2020: Interpretation of the spectrum of eastward-moving tropical convective anomalies. *Quarterly Journal of the Royal Meteorological Society*, **146** (727), 795–806, <https://doi.org/10.1002/qj.3709>.
- 224 Schreck, C. J., J. Molinari, and A. Aiyyer, 2012: A Global View of Equatorial Waves and Tropical Cyclogenesis. *Monthly Weather Review*, **140** (3), 774–788, <https://doi.org/10.1175/MWR-D-11-00110.1>.
- 227 Schreck, C. J., L. Shi, J. P. Kossin, and J. J. Bates, 2013: Identifying the MJO, Equatorial Waves, and Their Impacts Using 32 Years of HIRS Upper-Tropospheric Water Vapor. *Journal of Climate*, **26** (4), 1418–1431, <https://doi.org/10.1175/JCLI-D-12-00034.1>.
- 230 Straub, K. H., and G. N. Kiladis, 2003: The Observed Structure of Convectively Coupled Kelvin Waves: Comparison with Simple Models of Coupled Wave Instability. *Journal of the Atmospheric Sciences*, **60** (14), 1655–1668, [https://doi.org/10.1175/1520-0469\(2003\)060<1655:TOSOCC>2.0.CO;2](https://doi.org/10.1175/1520-0469(2003)060<1655:TOSOCC>2.0.CO;2).

- 234 Wallace, J. M., and V. E. Kousky, 1968: Observational evidence of kelvin waves in the
235 tropical stratosphere. *Journal of Atmospheric Sciences*, **25** (5), 900 – 907, [https://doi.org/10.1175/1520-0469\(1968\)025<0900:OEOKWI>2.0.CO;2](https://doi.org/10.1175/1520-0469(1968)025<0900:OEOKWI>2.0.CO;2).
- 236
- 237 Wheeler, M., and G. N. Kiladis, 1999: Convectively coupled equatorial waves: Analysis of clouds
238 and temperature in the wavenumber–frequency domain. *Journal of the Atmospheric Sciences*,
239 **56** (3), 374 – 399, [https://doi.org/10.1175/1520-0469\(1999\)056<0374:CCEWAO>2.0.CO;2](https://doi.org/10.1175/1520-0469(1999)056<0374:CCEWAO>2.0.CO;2).
- 240 Wheeler, M. C., and H. H. Hendon, 2004: An All-Season Real-Time Multivariate MJO Index:
241 Development of an Index for Monitoring and Prediction. *Monthly Weather Review*, **132** (8),
242 1917–1932, [https://doi.org/10.1175/1520-0493\(2004\)132<1917:AARMMI>2.0.CO;2](https://doi.org/10.1175/1520-0493(2004)132<1917:AARMMI>2.0.CO;2).